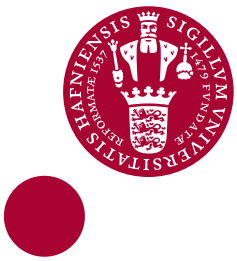

Photometric characterization of Lucideon and Avian Technologies color standards including application for calibration of the Mastcam-Z instrument on the Mars 2020 rover

Buz, Jennifer; Ehlmann, Bethany L.; Kinch, Kjartan Münster; Madsen, Morten Bo; Johnson, Jeffrey R.; Rice, Melissa S.; Maki, Justin; Bell, James F.

Published in:
Optical Engineering: The Journal of SPIE

DOI:
10.1117/1.OE.58.2.027108

Publication date:
2019

Document version
Publisher's PDF, also known as Version of record

Optical Engineering

OpticalEngineering.SPIEDigitalLibrary.org

Photometric characterization of Lucideon and Avian Technologies color standards including application for calibration of the Mastcam-Z instrument on the Mars 2020 rover

Jennifer Buz
Bethany L. Ehlmann
Kjartan Kinch
Morten Bo Madsen
Jeffrey R. Johnson
Melissa S. Rice
Justin Maki
James F. Bell, III

SPIE.

Jennifer Buz, Bethany L. Ehlmann, Kjartan Kinch, Morten Bo Madsen, Jeffrey R. Johnson, Melissa S. Rice, Justin Maki, James F. Bell, , III"Photometric characterization of Lucideon and Avian Technologies color standards including application for calibration of the Mastcam-Z instrument on the Mars 2020 rover," *Opt. Eng.* **58**(2), 027108 (2019), doi: 10.1117/1.OE.58.2.027108.

Photometric characterization of Lucideon and Avian Technologies color standards including application for calibration of the Mastcam-Z instrument on the Mars 2020 rover

Jennifer Buz,[a,*,†] Bethany L. Ehlmann,[a,b] Kjartan Kinch,[c] Morten Bo Madsen,[c] Jeffrey R. Johnson,[d] Melissa S. Rice,[e] Justin Maki,[b] and James F. Bell III[f]

[a]California Institute of Technology, Department of Geologic and Planetary Sciences, Pasadena, California, United States
[b]NASA Jet Propulsion Laboratory, La Cañada, California, United States
[c]University of Copenhagen, Niels Bohr Institute, Copenhagen, Denmark
[d]Johns Hopkins University Applied Physics Laboratory, Laurel, Maryland, United States
[e]Western Washington University, Geology Department, Physics and Astronomy Department, Bellingham, Washington, United States
[f]Arizona State University, School of Earth and Space Exploration, Tempe, Arizona, United States

Abstract. Several commercially available color standards exist, generated by a variety of manufacturers including LabSphere, Lucideon, and Avian Technologies. Previous work has characterized the photometric properties of LabSphere Spectralon targets. Here, we measure the visible and shortwave infrared (VSWIR; 0.4 to 2.5 μm) reflectance at multiple angles and determine the photometric properties of materials manufactured by Lucideon and Avian Technologies for potential use as calibration target materials for the Mars 2020 Mastcam-Z instrument. The Lucideon black, gray 33, green, and cyan samples are found to be significantly forward scattering. The yellow, red, and gray 70 samples are found to be weakly forward scattering. The Avian Technologies AluWhite98 sample was found to be weakly backward scattering. We characterize the absorptions observable and note the occurrence of wavelength-dependent photometric properties. The reflectance and photometric data collected and released here enable the use of these color standards for calibration of data from Mastcam-Z and other Mars-2020 rover instruments as well as provide key information for many other imaging and spectroscopy applications that require the calibration of data from multiple lighting or viewing geometries. [DOI: 10.1117/1.OE.58.2.027108]

Keywords: photometry; spectroscopy; calibration; Mars; color standards; reflectance.

Paper 181146 received Aug. 8, 2018; accepted for publication Jan. 15, 2019; published online Feb. 12, 2019.

1 Introduction

Calibration targets are essential in many applications for accurate radiometric calibration of data. Here, we describe the spectral and photometric properties of color standards from Lucideon and Avian Technologies, which we characterized prior to use on the Mars-2020 (M2020) rover mission. M2020 includes the Mastcam-Z (MCZ) instrument, which consists of a pair of multispectral, visible/near-infrared [VNIR, adjustable-zoom (focusable)] cameras. The science goals of the MCZ instrument, in brief, are to characterize the geomorphology and geology at the rover field site, assess current atmospheric and astronomical phenomena, and provide operational support and scientific context for the M2020 rover.[1]

The MCZ instrument includes two fixed calibration targets (primary and secondary) each composed of a reference set of color and grayscale materials of known spectral and photometric properties[1] (Fig. 1). Illumination conditions vary on the surface of Mars according to the local solar time and the aerosol opacity of the atmosphere at the time of observation. A calibration target is necessary for verification of the preflight calibration of the camera, monitoring the stability of the instrument throughout the mission, and conversion of the radiance measured in data numbers to radiance factor or Lambert albedo to enable comparison with laboratory reflectance spectra of Earth materials (e.g., Ref. 2). In addition, the MCZ calibration targets may be useful for calibration of other onboard instruments such as the VNIR (400 to 900 nm) and the shortwave infrared (SWIR; 1300 to 2600 nm) passive spectra from SuperCam, as well as engineering cameras and cameras mounted on the rover arm. Furthermore, the targets serve as a platform of known spectral characteristics to monitor dust deposition and removal throughout the mission (e.g., Refs. 3–5). For the calibration targets to enable these tasks, a detailed understanding of the photometric properties of the materials that compose the calibration targets is imperative. This is the goal of this study.

This study replicates some of the techniques and analyses conducted for the common reflectance standard, Spectralon® SRS-99 (Labsphere, North Sutton, New Hampshire).[6–8] The materials used here, manufactured by Lucideon (Staffordshire, United Kingdom) and Avian Technologies LLC (Sunapee, New Hampshire), are commercially available color standards. Therefore, we expect that the data acquired in this study will be of utility to others who employ these standards for imaging or spectroscopy applications or are evaluating them for potential use. We assess the

*Address all correspondence to Jennifer Buz, E-mail: jbuz@gps.caltech.edu

†Present Address: Northern Arizona University, Department of Physics and Astronomy, Flagstaff, Arizona, United States

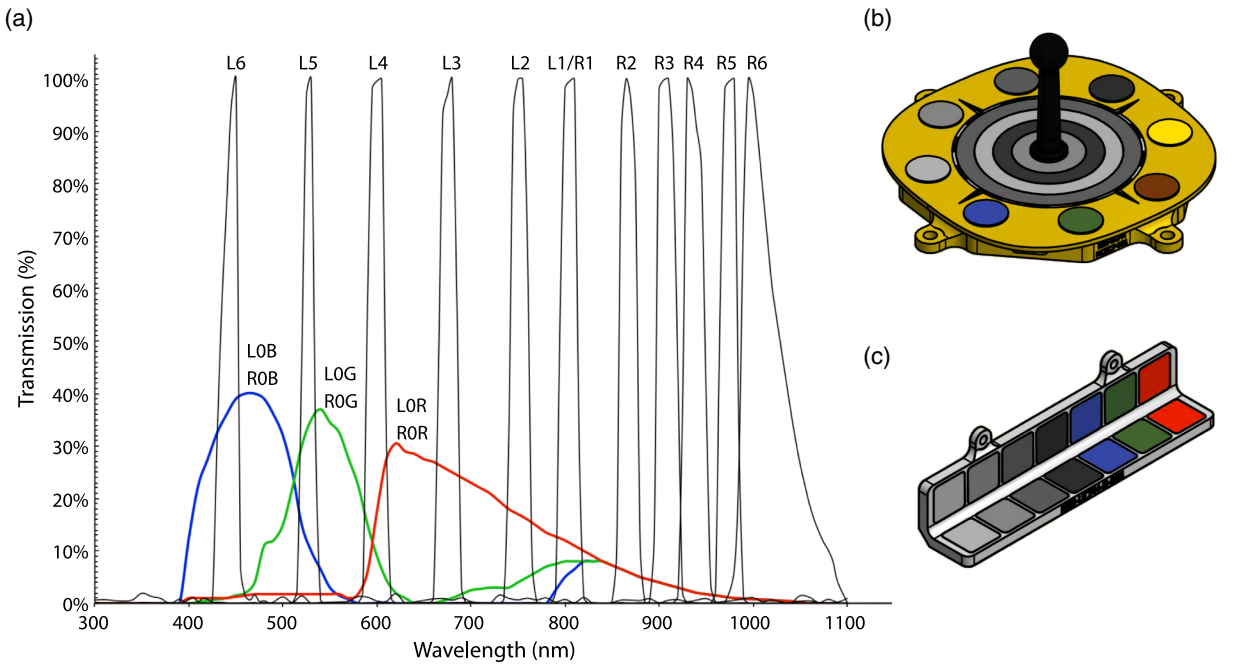

Fig. 1 (a) Preliminary estimates of MCZ filter transmission profiles. (b) Schematic of MCZ primary calibration target. Not shown, below each of the eight circular color and grayscale patches around the periphery lies a strong circular sweep magnet intended to minimize accumulation of Martian dust on the central part of these circular patches. (c) Secondary calibration target schematic.

wavelength-dependent spectroscopic properties and photometric behavior of the calibration materials (see data in Supporting Online Materials). This paper supplements detailed characterization of the actual assembled calibration targets and the derived bidirectional reflectance function (BRDF) for the calibration materials.

2 Mastcam-Z and its Calibration Targets

MCZ's Bayer-pattern CMOS detector and 12 filters [Fig. 1(a)] are used to measure the wavelength range of 445 to 1013 nm (preflight estimate) to discriminate iron-bearing minerals and certain water-bearing minerals by detection of their characteristic VNIR absorptions and/or spectral shapes.[9,10] For each camera, an additional solar filter with reduced transmission enables observation of the sun to determine atmospheric opacity. The primary MCZ calibration target is an ~8-cm-diameter disk with eight color/grayscale chips surrounding four concentric grayscale rings [Fig. 1(b)]. A gnomon is in the center of this calibration target. The gnomon casts a shadow across the calibration target that allows comparison of direct versus diffuse components of the solar and sky irradiance (e.g., Refs. 2 and 11). The calibration target is similar to those flown on the Mars Exploration Rovers (MERs) Spirit and Opportunity and on the Mars Science Laboratory (MSL) Curiosity rover with modifications based on lessons learned[1] and based on requirements for use of materials caused by instrumentation on board. Because the payload holds very sensitive instruments for remote detection of organic materials, silicone rubber–based materials such as those used as color references in previously flown calibration targets were avoided. The primary MCZ calibration target is mounted horizontally and located on the rover at a position where the MCZ instrument has an unobstructed view, where it will be fully illuminated during surface operations, and where there is a minimum of diffuse or reflected light from other structures on the rover. The target is viewed from the rover mast at an angle of 58 deg from vertical (emission angle = 58 deg), and geological materials on the surface are viewed at a wide range of angles. The secondary calibration target [Fig. 1(c)] is mounted on a vertical surface on the rover for monitoring of calibration targets at different angles and with different accumulation of dust.

Calibration procedures for the Mars2020 rover will be similar to those implemented on the MER and MSL missions. For each multispectral observation of the surface, a corresponding multispectral observation of the primary calibration target under similar illumination conditions will also be acquired.[2,12] From these calibration target images, regions of interest (ROIs) of uniform dust cover will be selected from each of the four grayscale rings and from the eight relatively dust-free central spots of the eight circles around the periphery. The ROI mean radiance values are plotted against laboratory-measured directional-hemispherical reflectance values of the calibration targets corrected for illumination and viewing geometry using their photometric properties.[5] To correct for the presence of dust, a two-layer scattering model is used, closely following that of Ref. 5 with a key difference in that all irradiance is assumed to come from the direction of the sun.[2] The result of this model is a conversion factor, which can be used to correct observed radiances from the Martian scene to radiance factor (I/F).[5] Lastly, the calibrated radiance factor can be divided by the cosine of the solar incidence angle to determine the relative reflectance, also known as $R*$ (REFF; see Sec. 3).[12–14] Given the range of possible illumination geometries, full knowledge of the photometric properties of calibration target materials is required to perform this analysis.

3 Methods

To characterize the photometric properties of the candidate MCZ calibration target materials, it was necessary to obtain reflectance measurements at a series of geometries with a stable and well-calibrated detector and light source. We used a multiwavelength spectrogoniometer developed at Caltech [Fig. 2(a)] that is capable of measuring at all azimuth (Az) angles (0 deg to 180 deg) and at emission (e) and incidence (i) angles from -70 deg to 70 deg with a minimum phase angle of ~ 12 deg. Incidence and emission angles are measured as positive angles from the vertical, and azimuth is measured positive clockwise from the horizontal projection of the incidence angle [Fig. 2(b)]. The phase angle (g), the angle between the incidence and emission angle, is calculated as follows:

$$g = \arccos[\cos(i) * \cos(e) + \sin(i) * \sin(e) * \cos(Az)].$$

The measurements were taken with an Analytical Spectral Devices FieldSpec 3®, which allows for reflectance measurements from 350 to 2500 nm through the use of a 512-element silicon array detector in the VNIR and two graded InGaAs photodiodes in the SWIR. These measurements are comparable to those taken with the Reflectance Experiment Laboratory (RELAB) instrumentation at Brown University.[15,16] The sample is illuminated with a halogen source with all other room lights turned off. Baffling ensures that the signal comes from a <7 mrad cone, corresponding to diameters on sample of <5 mm at $e = 0$ deg and <2 cm at $e = 70$ deg. Formally, this is a conical–conical reflectance (case 5, in Ref. 17) with small angles nearing the ideal BRDF. For a white reference standard, we used a Spectralon® target that is approximately Lambertian.[7–8] The Caltech goniometer was specifically designed for the Spectralon calibration target to lie coincident with the axes of rotation of the goniometer. To match this measurement plane, the MCZ calibration target reference materials were lifted using thin washers.

Prior to measurements, we optimized the gain on each detector with the Spectralon® present using a geometry of $i = 12$ deg and $e = 0$ deg. We then positioned the goniometer at the specified geometry and obtained a spectral average of 400 white reference measurements. (This includes a dark current measurement also using a 400 spectral average.) The reflectance of each candidate target material was then measured at this geometry, also using a 400 spectral average. Every 10 min the white reference was remeasured, and its spectrum saved.

To account for the differences in each detector, we used a routine available with the ASD FieldSpec 3® software. This routine uses five channels from each detector at the filter boundary to calculate a bias value for the VNIR and longer wavelength SWIR detectors. This bias value matches the offset with the shorter wavelength SWIR detector at the splice point.

Following Refs. 18 and 19, we output the reflectance as the reflectance factor (REFF) that is defined as follows:

$$\mathrm{REFF}(i, e, g, \lambda) = \frac{L_{\mathrm{samp}}(i, e, g, \lambda) - L_{\mathrm{dark}}(\lambda)}{L_{id}(i, e, g, \lambda) - L_{\mathrm{dark}}(\lambda)},$$

where $L_{\mathrm{samp}}(i, e, g, \lambda)$ is the radiance from the target measured at geometry (i, e, g) at a given wavelength, λ, $L_{id}(i, e, g, \lambda)$ is the radiance from an ideal, perfectly diffuse standard surface measured at geometry (i, e, g), and $L_{\mathrm{dark}}(\lambda)$ is the radiance measured with no incident light.

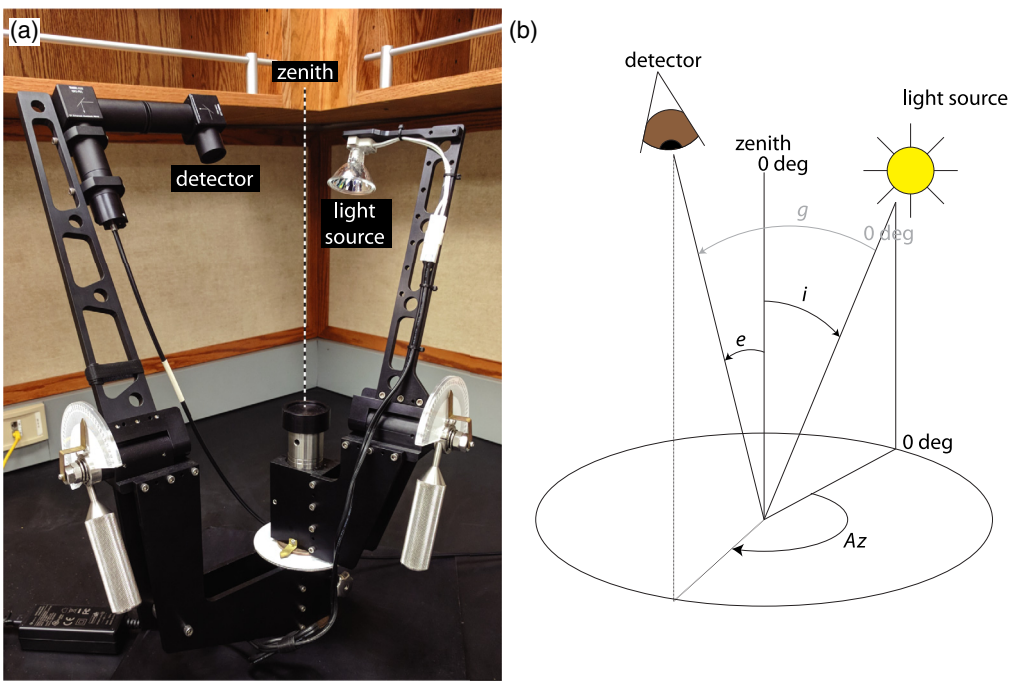

Fig. 2 (a) Goniometer set up at the Caltech Earth and Planetary Remote Sensing Laboratory. A fiber optic cable from the spectrometer is fed into the detector assembly. (b) Measurement convention used in this study. Arrows point in positive degree direction.

For this study

$$\mathrm{REFF}_{\mathrm{meas}}(i,e,g,\lambda) = \frac{L_{\mathrm{samp}}(i,e,g,\lambda) - L_{\mathrm{dark}}(\lambda)}{L_{\mathrm{std}}(i,e,g,\lambda) - L_{\mathrm{dark}}(\lambda)} R_{\mathrm{std}},$$

where $\mathrm{REFF}_{\mathrm{meas}}$ is the measured wavelength-dependent reflectance relative to the L_{std}, the Spectralon standard measured in the specified geometry. And R_{std} is the National Institute of Standards and Technology-certified value for the wavelength-dependent reflectance of Spectralon®.

Because the purpose of this study was to obtain an understanding of the photometric properties of the target materials, we obtained the REFF measurements at 76 geometries, illustrated in Fig. 3. To evaluate the scattering properties of the samples, we observed the change in REFF in- and out-of-plane at multiple geometries with $e = 58$ deg and $e = 30$ deg as well as for in-plane geometries at $e =$ 0 deg and $i = 30$ deg (Fig. 3). The emission angle of 58 deg was chosen because it is the approximate emission angle at which the MCZ detector will view the calibration target panel; $e = 30$ deg is a standard photometric study observation point and is similar to the path from the instrument to the secondary target ($e \cong 32$ deg). The remaining angles were chosen to provide a full-suite of measurement geometries enabling a characterization of the photometric properties. We assume symmetry in the photometric properties for azimuth angles 180 deg to 360 deg. Each measurement in this study includes the full spectral wavelength range of 350 to 2500 nm. The data were used to determine the wavelength-dependent reflectance of the calibration targets and their photometric properties, including characterization of wavelength-dependent changes in photometric behavior, which has been observed in prior studies of geological materials (e.g., Ref. 16). Modeling of Hapke parameters following Ref. 3 was attempted but produced poorly constrained fits and is not further discussed. Follow-up studies will obtain measurements of the targets at finer angular resolution but at limited wavelengths to determine the functional form of the BRDF.

To ensure that the sample holder material did not influence the spectra collected, we measured the sample holder material directly and noted its spectral properties (which were not in common with any of those of the target material and are not further discussed). Lastly, we confirmed absorptions and peaks in the 400- to 1100-nm range by measuring the samples using an Ocean Optics HR200CG ultraviolet-NIR Spectrometer at i and e of 0 deg.

4 Samples

Eight samples are candidate calibration target reference materials based on their ability to withstand the rover environment and their photometric properties. These samples are shown in Fig. 4 with the Spectralon® white reference also shown. The red, yellow, green, cyan, gray 33, gray 70, and black samples are manufactured by Lucideon while the AluWhite 98 (from now on referred to as white) target is manufactured by Avian Technologies LLC. The Lucideon targets are 5 cm × 5 cm glazed and matted aluminum silicate tiles. The white target is a 5.08 × 5.08 cm matte tile composed of sintered alumina.

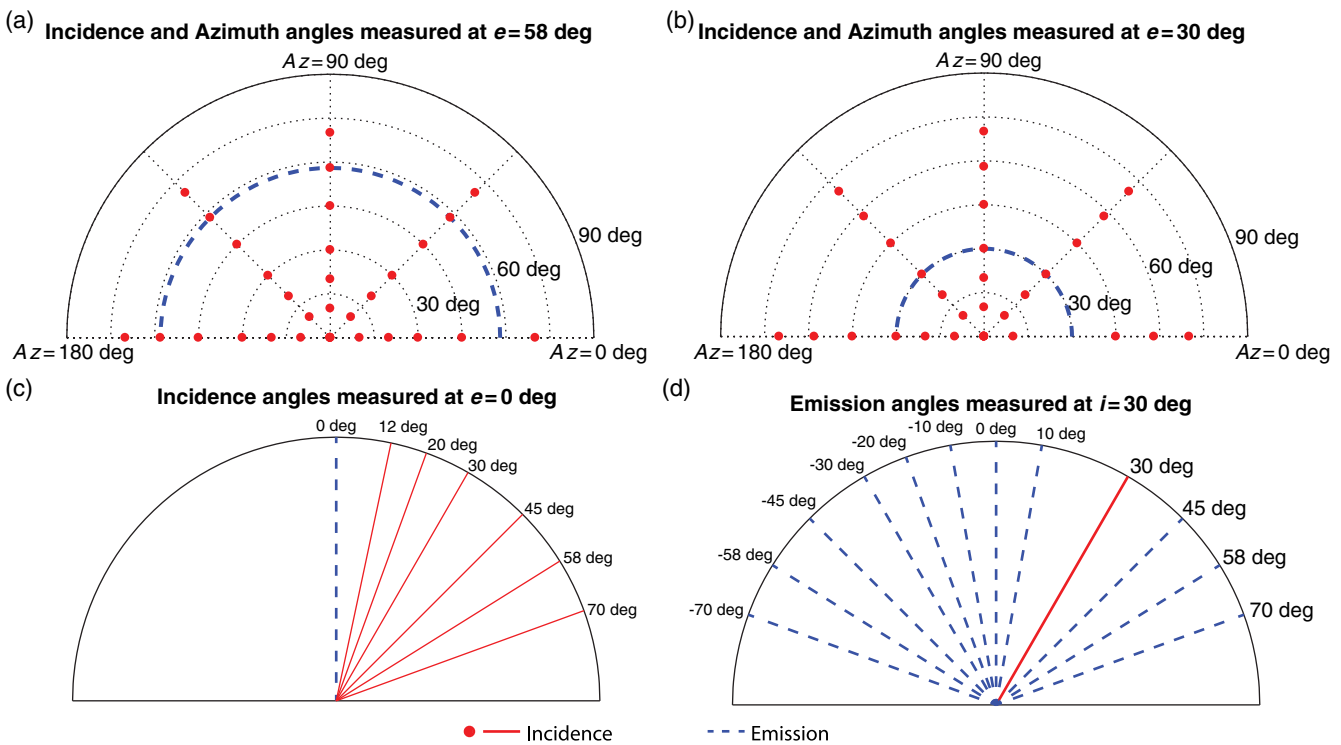

Fig. 3 Schematic showing the multiple measurement geometries acquired with the incidence angle indicated in red and the emission angle indicated in blue. Out-of-plane phase angle measurement geometries are shown in (a) and (b) where the emission angle is fixed and the incidence and azimuth angle vary. (c) and (d) The in-plane measurement geometries.

Fig. 4 Calibration targets used in this study with manufacturer indicated in parentheses and Spectralon® for comparison. All of the Lucideon targets are mounted on a black plastic holder. The white target is not mounted.

5 Results

5.1 *Data Quality Evaluation and Known Instrument Artifacts*

The Caltech goniometer data were examined in Ref. 16, compared to that acquired in RELAB, and matched within 10%. Comparison of our measurements on 5%, 20%, and 99% reflectance standards with Spectralon® calibration files provided by the manufacturer indicated correspondence within 5%, indicating no significant contribution from the light source, linear instrument response, and adequate instrument calibration. During our measurements, white reference spectra were acquired every 10 min to verify that the apparatus was stable. Data for wavelengths short of 400 nm and longer than 2500 nm were evaluated for quality and excluded due to low signal-to-noise ratio. The standard deviation REFF between 100 successive measurements (over ∼5 min) of Spectralon® is ≤0.012, indicating stability in the light source and instrument (Fig. 5). The 400- to 2500-nm wavelength range is reliable with the exceptions below where caution in interpreting data is needed.

In the raw data from the spectrometer and also occasionally in the corrected reflectance data, we observe spectral features at ∼1100 and ∼1320 nm (dashed gray lines in Fig. 5). According to correspondence with the makers of the ASD instrument, these absorptions are related to varying proportions of on-axis and off-axis signal entering the spectrometer, depending on brightness. These artifacts affect several of our spectra and are more pronounced at certain geometries. Consequently, the wavelength ranges 1100 ± 30 nm and 1320 ± 30 nm should be ignored in our REFF data. We also observe weak absorptions at ∼1400 nm and ∼1900 nm (dashed blue lines in Fig. 5), which can be caused by vibrational absorptions related to water in the instrument path length. In most REFF data, this wavelength region is reliable. There are strong 1400 and 1900 nm absorptions in the samples themselves due to water in the materials; however, smaller, superimposed fluctuations should be interpreted with caution.

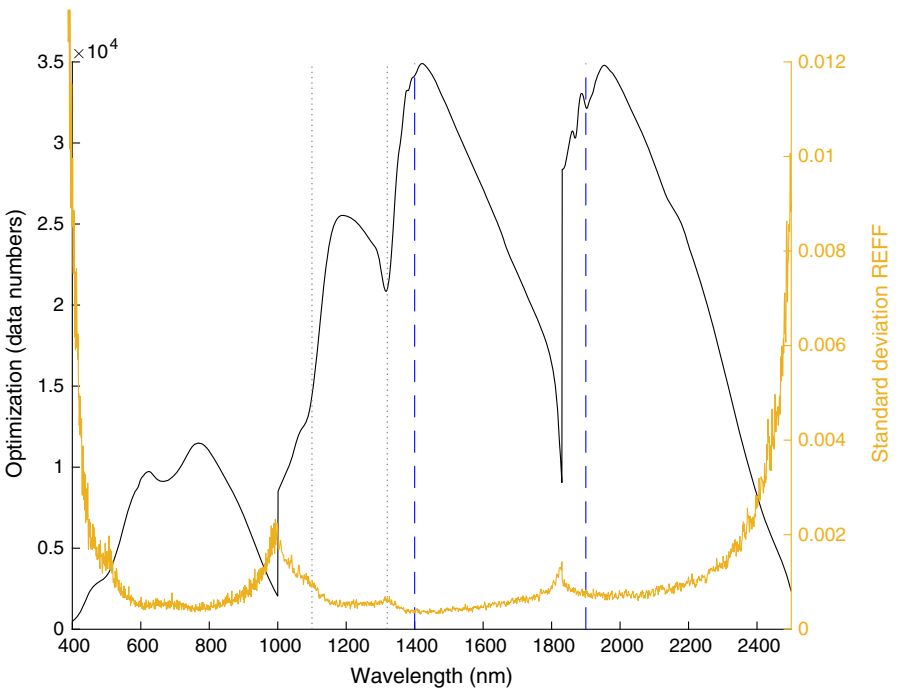

Fig. 5 Optimized instrument response for the three detectors of the ASD FieldSpec 3® exhibiting features at 1100 and 1320 (dotted gray lines) that should be interpreted as measurement artifacts and 1400 and 1900 nm from water (dashed blue lines) that should be interpreted with caution. Incidence angle was 12 deg and emission angle 0 deg. Standard deviation REFF for 100 successive Spectralon® measurements are shown in orange with corresponding right axis.

5.2 *Target Spectral and Photometric Properties*

A summary of the spectral and photometric properties of the target materials is given in Table 1. The most illustrative BRDF measurement results are given in Figs. 6 and 7; all data and normalization plots are available in the supplementary materials.

All targets demonstrate some absorptions in the 400-2400 nm range (Fig. 6). All absorptions shortward of 1000 nm are broad absorptions that control the target color properties. At longer wavelengths, all samples except the gray and black samples exhibit absorptions at 1900 nm due to water. The white, yellow, and red targets exhibit 1400 nm features due to water, and the yellow and red even have small overtones at 940 and 1120 nm related to molecular water. The white and four color targets also exhibit an absorption at 2200 nm due to Si-OH or Al-OH. Additionally, the white sample has a 694-nm peak [Fig. 6(h)] that was confirmed with the UV-NIR spectrometer and corresponds to a well-documented fluorescence in chromium,[20] a common substitution in Al_2O_3, of which the white target is composed. It may be related to a Cr for Al substitution in the structure.

The black, gray 33, green, and cyan samples are significantly forward scattering at 800 nm, i.e., >200% change in reflectance over the angles measured. The yellow, red, and gray 70 samples are quasi-isotropic but weakly forward scattering at 800 nm. The white sample is quasi-isotropic but weakly back scattering at 800 nm (Fig. 6). All the samples exhibited wavelength-dependent photometric properties, some of which were quite significant (Fig. 7; Table 1). The red, yellow, green, blue, and black samples were more forward scattering at short wavelengths and become significantly less forward scattering at longer wavelengths. The gray 33 and gray 70 samples were found to be less forward scattering at shorter wavelengths. For all samples except white, measurements made at phase angles ~103 deg and ~112 deg [arrows in Fig. 7(a)] deviate from the general upward trend of greater normalized REFF with larger phase angle (these measurements were verified by repeat measurements).

5.3 *Convolution to MCZ Filter Set*

We approximated the MCZ camera multispectral data of the calibration target reference materials (Fig. 8) by integrating the full-resolution spectra over MCZ filter transmission profiles [Fig. 1(a)]. At the time of this work, the MCZ filters had not been manufactured and verified, and thus the MCZ profiles were estimated as the replicas of the Mastcam filter transmission profiles.[21] The profile of the Mastcam 805 nm filter was duplicated and shifted to create hypothetical bandpasses for the ~600 and ~975 nm filters that are new to MCZ. Overall, the MCZ filter set reproduces the general spectral shape of the targets.

5.4 *Slope as a Function of Viewing Geometry*

There is a significant change in spectral slope with viewing geometry for certain measurement suites (Fig. 9). The degree of this change is variable across samples and measurement suites. As an example, Fig. 9 demonstrates two measurement suites for the gray 33 and yellow samples. The yellow sample appears to have little to no change in spectral slope for either measurement suite. The gray 33 sample, however, has significant change in spectral slope at the $Az = 180$, $e = 58$ measurement suite, i.e., at higher phase angle. This effect is still observed, though to a lesser degree at the $e = 30$

Table 1 Summary of spectral and photometric properties for MCZ calibration target reference materials.

Sample	Absorptions (nm)[a]	Other spectral features	Scattering behavior at 800 nm	ΔREFF at 400 nm (%)[b]	ΔREFF at 800 nm (%)[b]	ΔREFF at 2400 nm (%)[b]
Lucideon red	1400, 1900, 2200	Sharp increase in REFF between 575 and 700 nm	Quasi-isotropic (weak forward)	483	125	134
Lucideon yellow	**570, 630, 800,** 1400, 1500, 2900	Sharp increase in REFF between 475 and 575 nm	Quasi-isotropic (weak forward)	580	132	142
Lucideon green	**400, 650, 800,** 1500, 1900, 2200	Overall shape from broad absorptions	Forward	373	274	139
Lucideon cyan	**650, 800**, 1500, 1900, 2200	Overall shape from broad absorptions	Forward	204	315	145
Lucideon gray 33	**500, 600, 650**	Decrease in REFF beyond 700 nm	Forward	200	210	612
Lucideon gray 70	**600, 650**	Decrease in REFF beyond 700 nm	Quasi-isotropic (weak forward)	125	128	242
Lucideon black	1650	Increase in REFF between 700 and 1300 nm and beyond 1650 nm	Forward	654	673	205
Avian Technologies AluWhite 98	**450**, 1900, 2200	Sharp peak at 698 nm	Quasi-isotropic (weak backward)	67	70	75

[a]Absorptions in bold occur within MCZ filter range.
[b]Percentage change in REFF from the minimum phase angle (12 deg) to maximum phase angle (128 deg) at the specified wavelength.

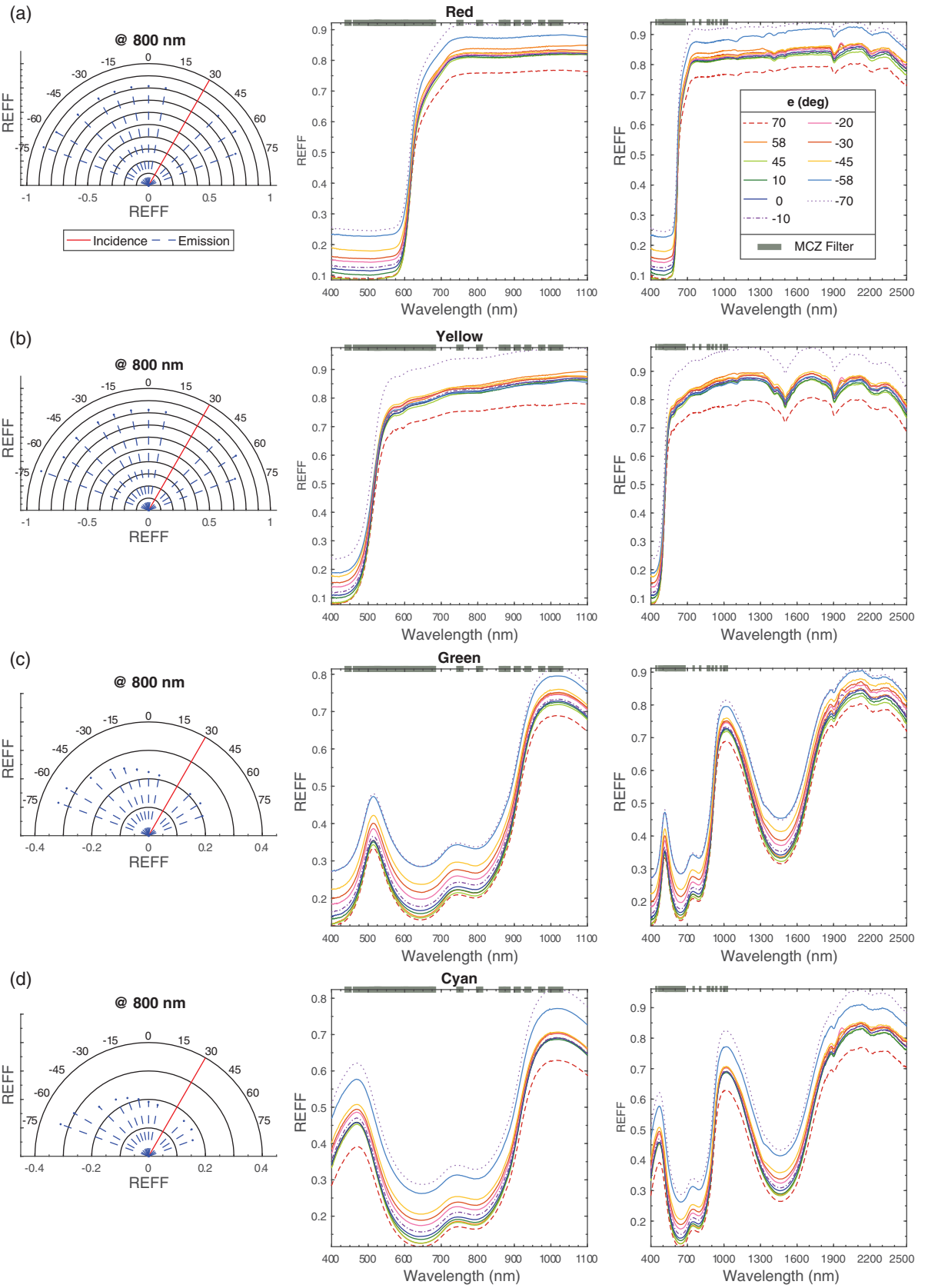

Fig. 6 Spectra and scattering properties of the MCZ calibration target reference materials. The left most polar diagrams show the effect of changing emission angle on the REFF at 800 nm for a fixed incidence angle of 30 in the principal plane. If the sample were isotropic its changing angular REFF would follow the semicircle. The right two columns show the spectra for the various samples at $Az = 0$ deg and $i = 30$ deg. The middle column shows only the MCZ relevant wavelengths, and the right column shows the full measurement range. (a) Red, (b) Yellow, (c) Green (d) Cyan, (e) Gray 33, (f) Gray 70, (g) Black, and (h) White.

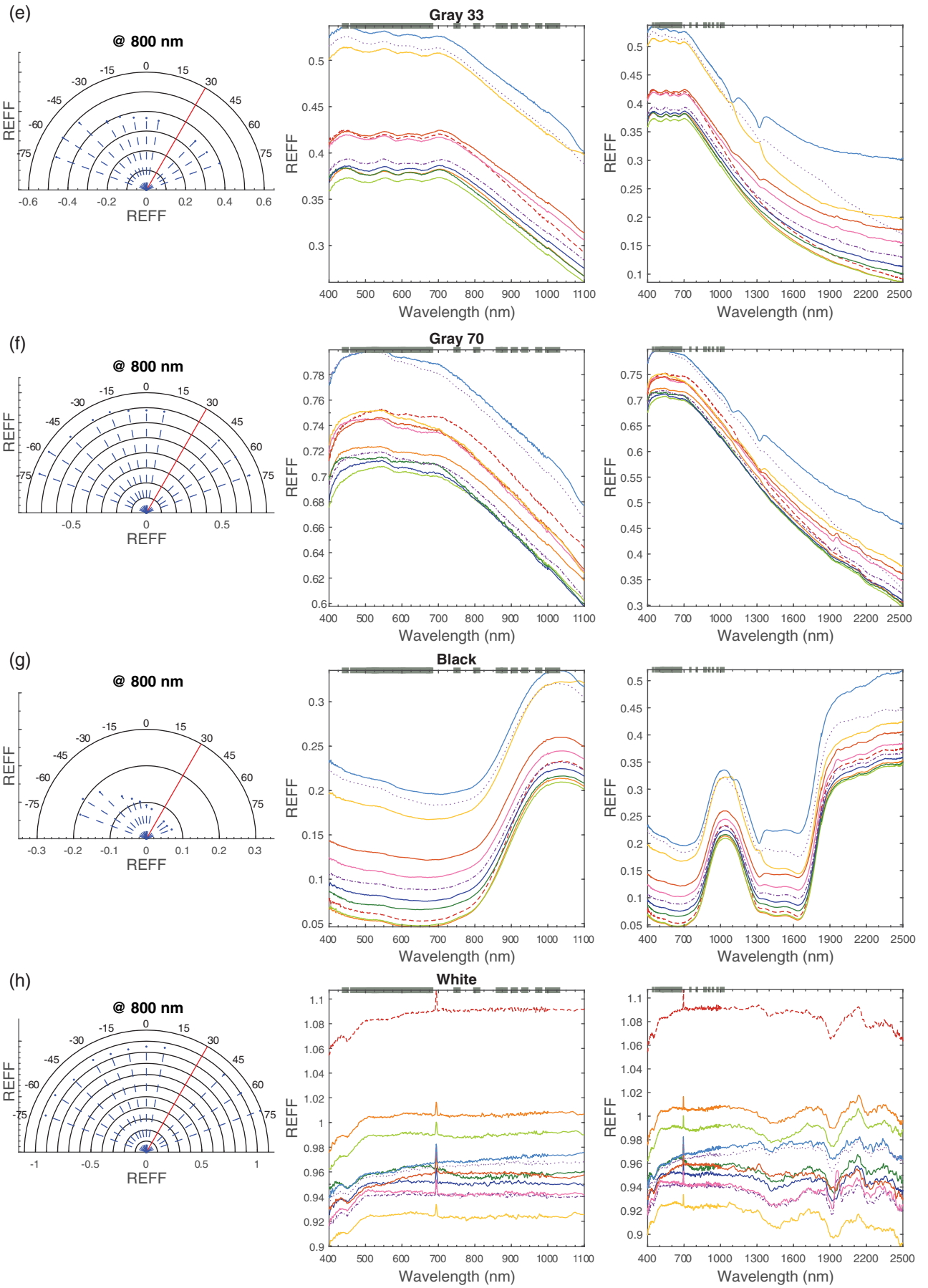

Fig. 6 (continued).

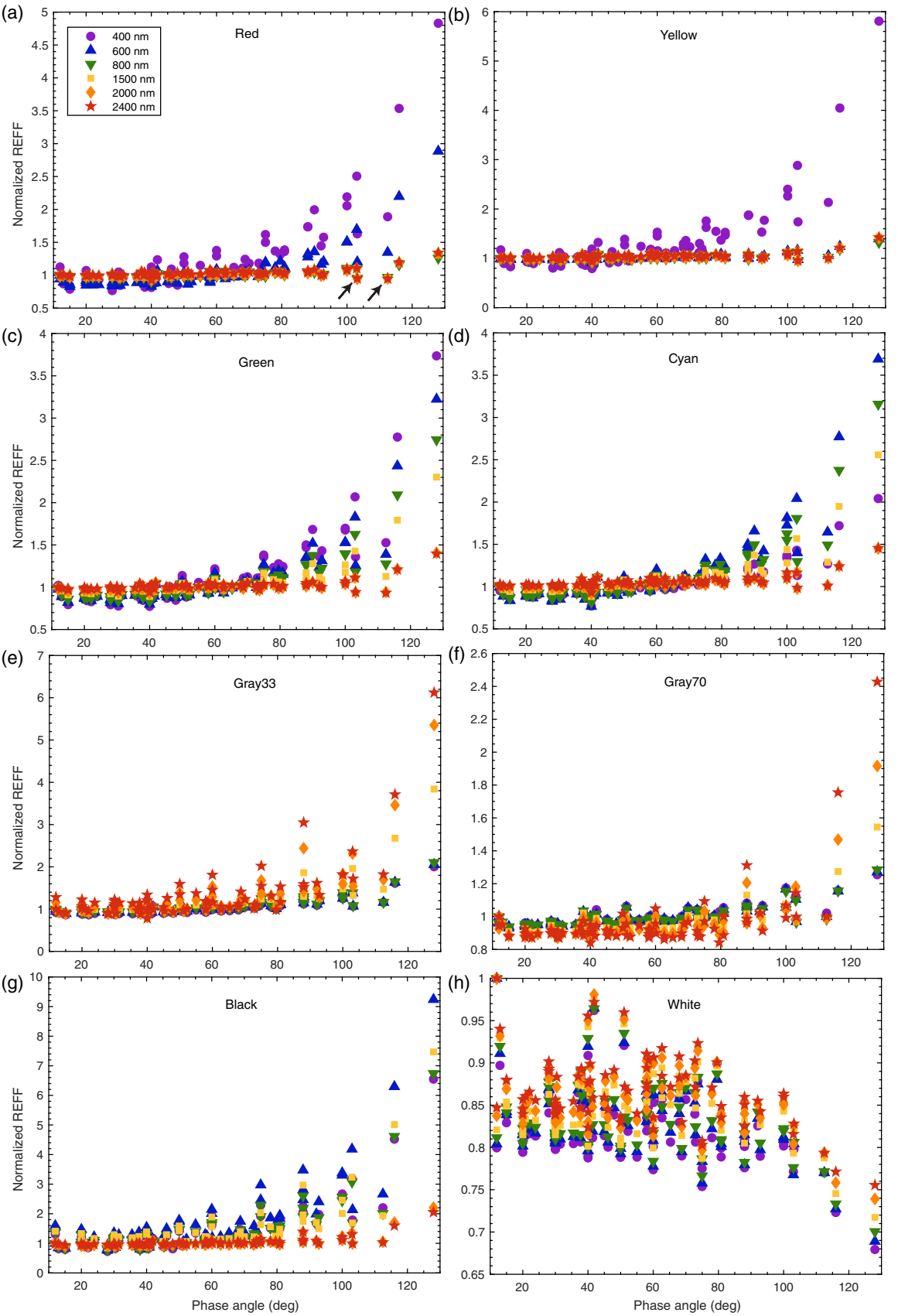

Fig. 7 REFF at 400, 600, 800, 1500, 2000, and 2400 nm for all measured geometries normalized to REFF value at $g = 12$ deg. All samples except white demonstrate a positive trend with increasing phase angle, indicating forward scattering behavior. White displays a weak negative trend with phase angle indicating backward scattering behavior. There is a shallowing of this trend for the longer wavelength measurements. (a) Red, (b) Yellow, (c) Green (d) Cyan, (e) Gray 33, (f) Gray 70, (g) Black, and (h) White.

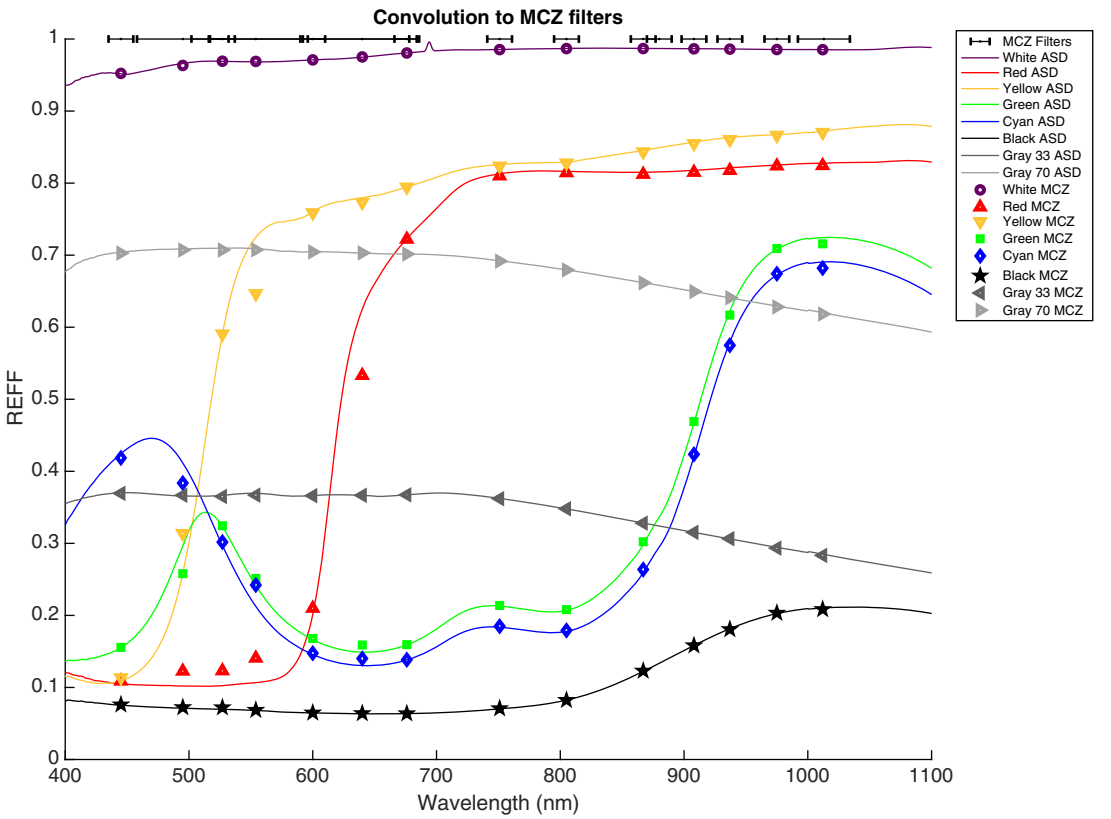

Fig. 8 Convolution of spectra on calibration target materials to MCZ filter set.

suite. This is likely due to wavelength-dependent photometric properties indicated by the data in Fig. 7. We examined the whole dataset, and the green, black, and gray 33 samples exhibit significant changes in slope with viewing geometry, whereas the rest exhibit this effect to a lesser extent. There is no consistent change in slope with viewing geometry observed in the white sample. The reader may visualize these with data available in the supplementary materials.

5.5 *Change in Absorption Strength as a Function of Viewing Geometry*

Two absorptions were analyzed for changes in band depth with viewing geometry: the 1470-nm absorption band on the green sample and the 660-nm absorption band on the gray 33 sample (Fig. 10). As an example, on the green sample, the band depth decreases with increasing phase angle. The sample, however, is strongly forward scattering as previously mentioned, so there is also an increase in REFF with phase angle. There is no observable trend with absorption strength for the gray 33 sample. All samples with wavelength-dependent photometric properties (Fig. 10) can exhibit these band depth changes, which can be examined in detail with data in the supplementary material.

6 Discussion

For some applications where photometry is important, such as in observations of materials on Mars with the Mars2020 rover, this study shows that the characterization of the angular dependence of sample reflectance for these candidate calibration target materials is critical. The suite of targets do not all behave in the same manner with weakly backward scattering (white), weakly forward scattering (yellow, red, and gray 70), and strongly forward scattering (cyan, green, gray 33, and black) behavior, depending on the sample and the wavelength of measurement. Just as with the RTV materials (pigmented synthetic silicone rubber) used in calibration targets flown on earlier missions to Mars, these calibration target materials are not Lambertian. Several of these vary significantly from isotropic behavior, but their photometric properties vary in consistent ways that can be described. Additionally, none of the targets show significant specular behavior.

When compared with the calibration targets found on the MER rover calibration target and MSL Curiosity's Mastcam calibration targets,[2,11] these candidate materials from commercial vendors are spectrally flatter in the 400- to 700-nm range, with the exception of the green target. Sharp absorptions should be avoided in calibration target materials, especially if they occur near the boundaries of the bandpass filters, but these targets have smoothly varying properties in the relevant 400- to 1100-nm range for Mars2020/MCZ and for any other VNIR imaging and spectroscopy investigations. The change in photometric properties with wavelength for each target provides an explanation for why changes in slope and absorption strength are observed in the samples with changes in viewing geometry. For analysis of spectra, this highlights why correction for calibration target photometric properties are crucial as the sun angle on the calibration target varies.

The white emission peak at 698 nm is an interesting, unexpected exception, but as it occurs within the center of the bandpass and is relatively small, it should not affect

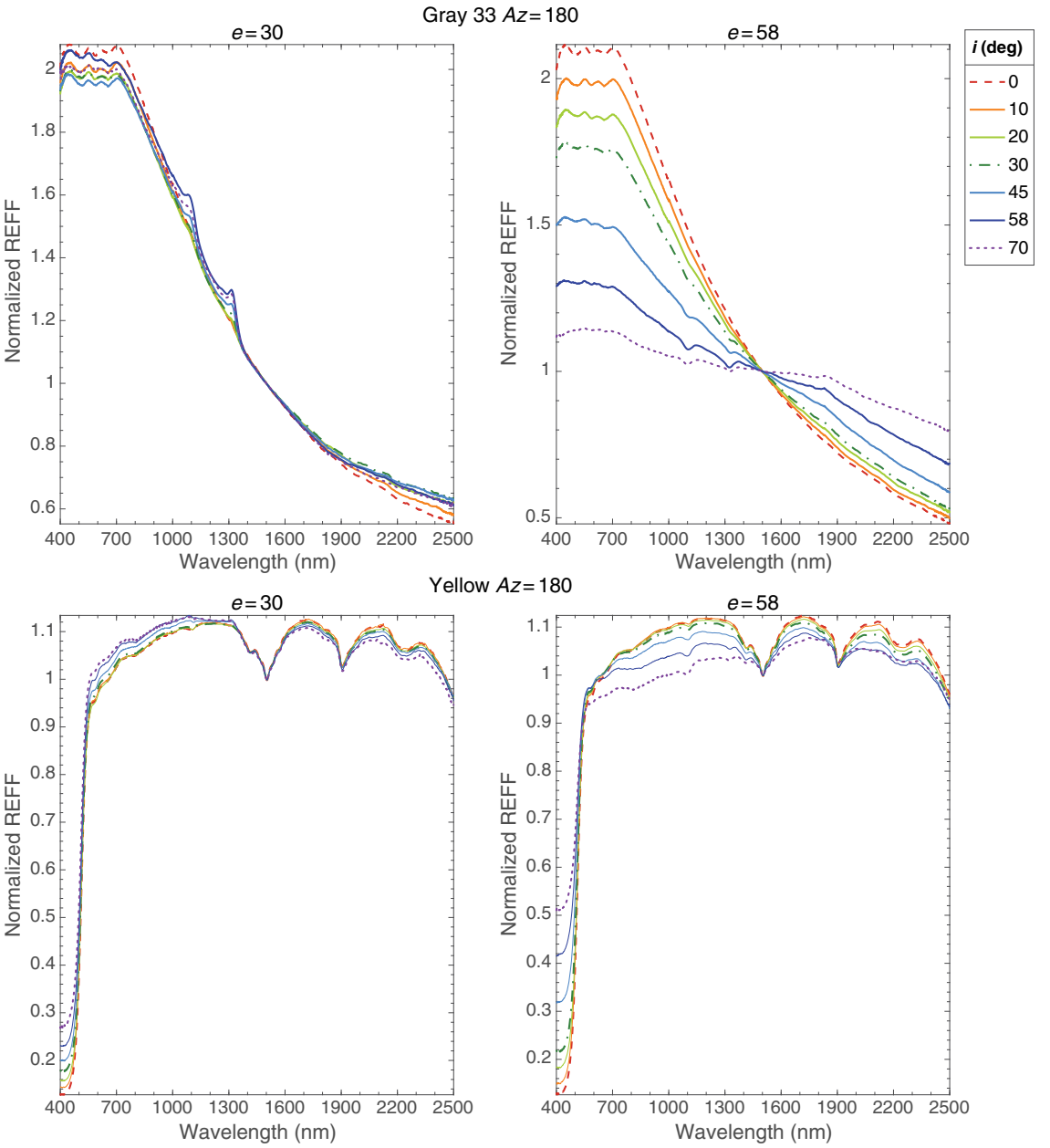

Fig. 9 Slope as a function of viewing geometry for the same set of measurements for gray 33 and yellow samples at $Az = 180$, normalized to REFF at 1500 nm. (left) MCZ relevant wavelengths, (right) full wavelength range, (top) Gray 33, and (bottom) Yellow.

calibration. Sharp absorptions are present at longer wavelengths in the red, yellow, green, cyan, and white calibration materials tested, so users for SWIR multispectral imaging applications should consider these when selecting calibration materials and bandpass cutoffs. The emission peak in white and the sharp absorptions at larger wavelengths may provide additional information to characterize wavelength position. On the other hand, because several sharp absorptions are due to bound water in the sample, it is possible that they will weaken or shift a few 10's of nm due to changing absorption shape with reduced water content under low Martian pressure or vary as a function of time of day (due to changes in relative humidity, Refs. 22 and 23). For observations at longer wavelengths than the MCZ instrument, e.g., by SuperCam on Mars, the narrow absorptions confound use as uniform surfaces but may prove useful for monitoring dust buildup (by absorption shallowing), complementing short wavelength observations.

The downward trending REFF measurements at phase angles ~103 and ~112 may be due to internal instrument effects (i.e., related to on and off axis light) or may be manifestations of actual scattering properties of the targets. With this data set, it is not possible to distinguish between these scenarios.

7 Conclusions and Future Work

The measurement suite captures the effect of viewing geometry on REFF for one Avian Technology target (AluWhite98) and seven Lucideon targets (red, yellow, cyan, green, gray 70, gray 33, and black), characterizing their photometric properties. Some of the samples are quasi-isotropic: the white target

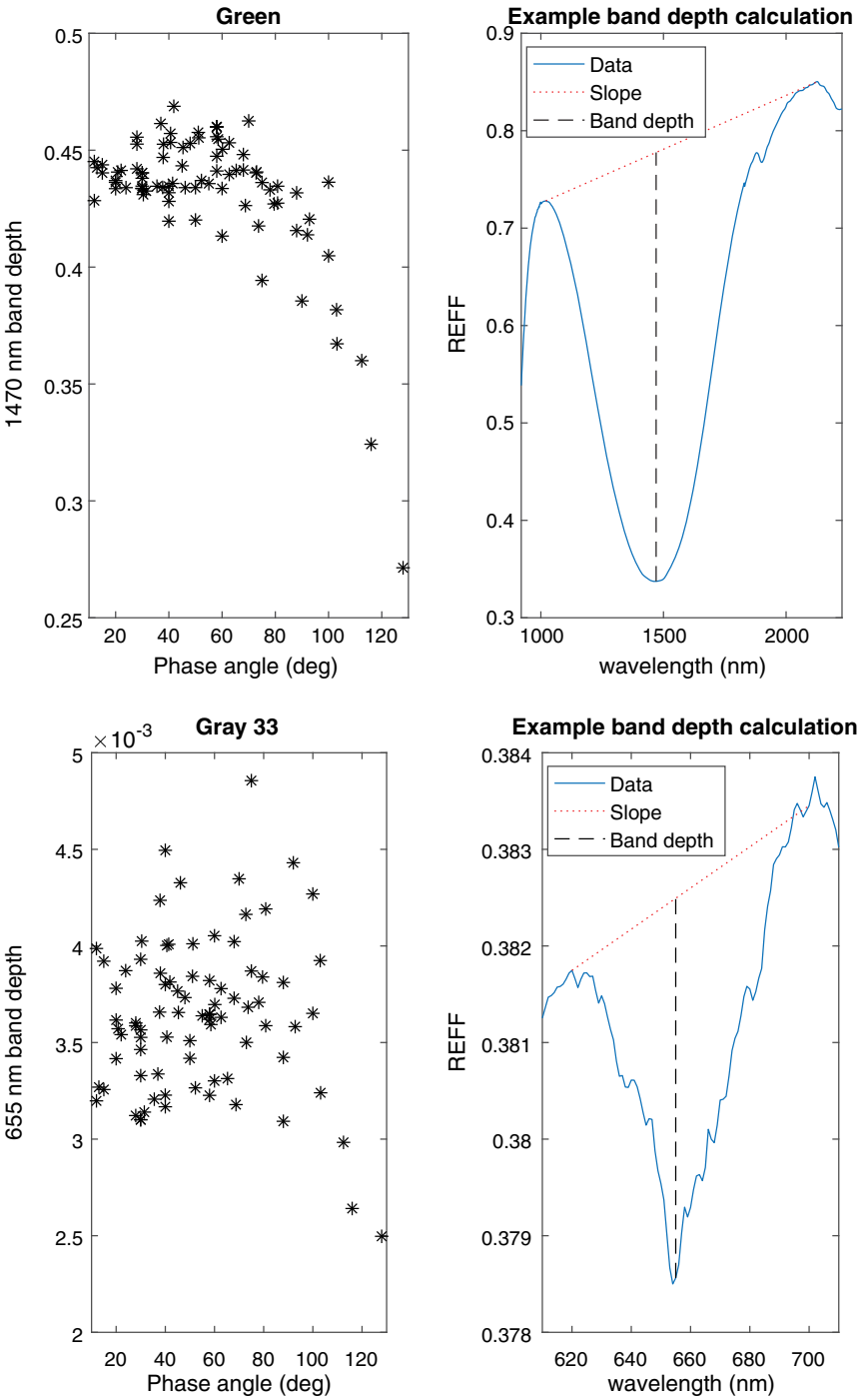

Fig. 10 Band depth calculations and changes with phase angle. (left) Band depths at all phase angles, (right) Example band depth calculation, (top) Green 1470 nm absorption, and (bottom) Gray 33 655 nm absorption.

is slightly backward scattering and the red, yellow, and gray 70 targets are slightly forward scattering. The cyan, green, gray, and black targets are strongly forward scattering. The forward scattering behavior is most significant at shorter wavelengths (i.e., in the MCZ measurement range) and for all samples except the gray samples, decreases at longer wavelengths. This wavelength dependence causes changes in spectral slope and absorption band depth depending on the viewing geometry. The scattering properties have been quantified here and can thus be corrected for. Our data alone are too sparse for a full BRDF characterization as was done in Ref. 11, but this will be future work at a more restricted set of wavelengths. Additional measurements will be taken at the Bloomsberg University Goniometer, and the data will be integrated into a scattering model covering all geometries.

Acknowledgments

Dataset and additional figures are available at https://doi.org/10.22002/D1.1154. JB thanks Dr. Ed Cloutis for early discussions related to this study and Dr. Will Grundy for

assistance in development and implementation of attempted photometric models. MBM gratefully acknowledges supporting grant CF16-0981, which covered salary for KK but also purchase of the calibration target references used in this study. This work was funded by a Mars-2020, Mastcam-Z grant to BLE, and a NASA Earth and Space Sciences Fellowship #NNX15AQ95H partially supported JB.

References

1. J. F. Bell et al., "MastCam-Z: designing a geologic, stereoscopic, and multispectral pair of zoom cameras for the NASA Mars 2020 rover," in *3rd Int. Workshop on Instrum. for Planet. Missions*, Pasadena, California (2016).
2. J. F. Bell et al., "The Mars science laboratory curiosity rover Mastcam instruments: preflight and in-flight calibration, validation, and data archiving," *Earth Space Sci.* **4**, 396–452 (2017).
3. J. R. Johnson et al., "Radiative transfer modeling of dust-coated Pancam calibration target materials: Laboratory visible/near-infrared spectrogoniometry," *J. Geophys. Res.* **111**(E12) (2006).
4. K. M. Kinch et al., "Dust deposition on the Mars Exploration Rover Panoramic Camera (Pancam) calibration targets," *J. Geophys. Res.* **112**(E6) (2007).
5. K. M. Kinch et al., "Dust deposition on the decks of the Mars Exploration Rovers: 10 years of dust dynamics on the Panoramic Camera calibration targets," *Earth Space Sci.* **2**, 144–172 (2015).
6. C. J. Bruegge et al., "Use of spectralon as a diffuse reflectance standard for in-flight calibration of earth-orbiting sensors," *Opt. Eng.* **32**, 805–814 (1993).
7. S. P. Flasse et al., "Modeling spectralon's bidirectional reflectance for in-flight calibration of Earth-orbiting sensors," in *Recent Adv. in Sens., Radiometric Calibration, and Process. of Remotely Sensed Data*, Orlando, Florida (1993).
8. C. Bruegge, N. Chrien, and D. Haner, "A spectralon BRF data base for MISR calibration applications," *Rem. Sens. Environ.* **77**, 354–366 (2001).
9. R. G. Burns, *Mineralogical Applications of Crystal Field Theory*, Vol. **5**, Cambridge University Press, Cambridge (1993).
10. R. N. Clark et al., *USGS Digital Spectral Library splib06a*, US Geological Survey, Reston, Virginia (2007).
11. J. F. Bell et al., "Mars Exploration Rover Athena Panoramic Camera (Pancam) investigation," *J. Geophys. Res-Planet.* **108**, 8063 (2003).
12. D. F. Wellington et al., "Visible to near-infrared MSL/Mastcam multispectral imaging: Initial results from select high-interest science targets within Gale Crater, Mars," *Am. Mineral.* **102**, 1202–1217 (2017).
13. B. Hapke, *Theory of Reflectance Spectroscopy*, Cambridge University Press, Cambridge (1993).
14. R. J. Reid et al., "Imager for Mars Pathfinder (IMP) image calibration," *J. Geophys. Res.* **104**, 8907–8925 (1999).
15. J. F. Mustard and C. M. Pieters, "Photometric phase functions of common geologic minerals and applications to quantitative-analysis of mineral mixture reflectance spectra," *J. Geophys. Res-Solid* **94**, 13619–13634 (1989).
16. C. Pilorget et al., "Wavelength dependence of scattering properties in the VIS-NIR and links with grain-scale physical and compositional properties," *Icarus* **267**, 296–314 (2016).
17. G. Schaepman-Strub et al., "Reflectance quantities in optical remote sensing—definitions and case studies," *Remote Sens. Environ.* **103**, 27–42 (2006).
18. United States National Bureau of Standards and F. E. Nicodemus, *Geometrical Considerations and Nomenclature for Reflectance*, Vol. **160**, US Department of Commerce, National Bureau of Standards, Washington (1977).
19. Analytical Spectral Devices, *FieldSpec Pro–User's Guide*, Analytical Spectral Devices, Boulder, Colorado (2002).
20. D. D. Ragan, R. Gustavsen, and D. Schiferl, "Calibration of the ruby R1 and R2 fluorescence shifts as a function of temperature from 0 to 600 K," *J. App. Phys.* **72**, 5539–5544 (1992).
21. M. C. Malin et al., "The Mars Science Laboratory (MSL) Mast cameras and Descent imager: Investigation and instrument descriptions," *Earth and Space Sci.* **4**, 506–539 (2017).
22. J. L. Bishop and C. M. Pieters, "Low-temperature and low atmospheric pressure infrared reflectance spectroscopy of Mars soil analog materials," *J. Geophys. Res.* **100**(E3), 5369–5379 (1995).
23. E. A. Cloutis et al., "Spectral reflectance properties of minerals exposed to simulated Mars surface conditions," *Icarus* **195**(1), 140–168 (2008).

Jennifer Buz is a postdoctoral scholar at Northern Arizona University. Her research focuses on remote sensing, spectroscopy, mineralogy, geology, magnetism, and surface properties of the terrestrial planets. Her work involves the use of data acquired by planetary satellites as well as laboratory analyses on extraterrestrial materials such as Martian metetorites and Apollo samples. She is a member of the Mars Science Laboratory Curiosity rover science team and is involved with the Mars 2020 rover Mastcam-Z instrument.

Bethany L. Ehlmann is a professor of planetary science at Caltech and Research Scientist at NASA's Jet Propulsion Laboratory. Her research focuses on the mineralogy and chemistry of planetary surfaces, remote sensing techniques and instruments, astrobiology, and science policy, and outreach. She is a member of the science teams for the Mars Exploration Rovers (Spirit and Opportunity), the CRISM imaging spectrometer for Mars, the Mars Science Laboratory Curiosity rover, and the upcoming Mars 2020 rover.

Kjartan Kinch is a physicist and planetary scientist at the Niels Bohr Institute of Copenhagen University. He has worked extensively on reflectance calibration and dust correction for multispectral Mars rover cameras on the Mars Exploration Rovers and Mars Science Laboratory missions. He is a coinvestigator on the Mastcam-Z camera on the Mars 2020 rover mission and is the lead designer of the Mastcam-Z radiometric calibration target.

Morten Bo Madsen is a physicist at the Niels Bohr Institute at University of Copenhagen. He has a broad interest in the exploration of Mars and worked on five landed missions on the planet. He is coinvestigator on the Mastcam-Z, SuperCam, and MOXIE experiments on NASA's Mars 2020 rover. Scientific achievements include identification of the source of magnetism of Martian dust and soil; participation in proving presence of water ice in the Martian subsurface.

Jeffrey R. Johnson is a principal professional scientist at the Johns Hopkins University Applied Physics Laboratory. Currently, he is an associate principal investigator and participating scientist for the Mars Exploration Rover Opportunity, a participating scientist on the Mars Science Laboratory Curiosity, and a coinvestigator on the SuperCam and Mastcam-Z instruments on the Mars2020 mission. He serves as the chair of the Mars Exploration Program Analysis Group (MEPAG) and is an associate editor for Icarus.

Melissa S. Rice is an assistant professor of planetary science at Western Washington University, where she has a joint appointment in the geology department and the physics and astronomy department. Her research focuses on the sedimentology, stratigraphy, and mineralogy of Mars. She is a collaborator on the active Mars Exploration Rover Opportunity missions, a participating scientist on the Mars Science Laboratory rover mission, and a coinvestigator for the Mastcam-Z instrument for the Mars2020 rover mission.

Justin Maki specializes in the development and operation of imaging systems for NASA planetary missions at the Jet Propulsion Laboratory/California Institute of Technology, in Pasadena, CA. He is the lead coinvestigator for the Mars InSight cameras, the imaging scientist for the Mars 2020 Rover mission, and deputy principal investigator for the Mars 2020 Mastcam-Z investigation. Previous NASA project involvement includes Cassini, Mars Pathfinder, Mars Exploration Rover, and the Mars Science Laboratory Rover missions.

James F. Bell III is a professor in the School of Earth and Space Exploration at Arizona State University in Tempe, Arizona, an adjunct professor in the Department of Astronomy at Cornell University in Ithaca, New York, and a Distinguished Visiting Scientist at NASA's Jet Propulsion Laboratory in Pasadena, California. His research primarily focuses on the geology, geochemistry, and mineralogy of planets, moons, asteroids, and comets using data obtained from telescopes and spacecraft missions.